



Enhancing Activity, Charge Transport, Power Production, and Stability of Commercial Solid Oxide Fuel Cells with Yttria-Stabilized Zirconia Nanoparticles

Sixbert P. Muhoza, ^{1,2,3} Shiwoo Lee, ^{1,4} Xueyan Song, ^{1,5,*} Bo Guan, ^{1,5} Tao Yang, ^{1,2} and Michael D. Gross ^{1,2,3,*,z}

Interconnected networks of 10–30 nm yttria-stabilized zirconia (YSZ) nanoparticles dramatically enhance both the electrocatalytic activity and bulk charge transport of commercial lanthanum strontium manganite (LSM)-YSZ solid oxide fuel cell (SOFC) cathodes. The improvement in both electrode functions increases the maximum power density of the commercial SOFC by 90%. In comparison, modifying cathodes with lanthanum strontium cobalt ferrite (LSCF) and praseodymium barium cobaltite (PBC) nanoparticles, highly active catalysts with mixed ionic-electronic conductivity (MIEC), only enhances electrocatalytic activity. The combination of dual enhanced electrode functions with nanoYSZ results in a maximum power density that is 50% and 11% higher than LSCF and PBC, respectively. Finally, the performance stability over time is highest for nanoYSZ modified cells.

© 2020 The Author(s). Published on behalf of The Electrochemical Society by IOP Publishing Limited. This is an open access article distributed under the terms of the Creative Commons Attribution 4.0 License (CC BY, http://creativecommons.org/licenses/by/4.0/), which permits unrestricted reuse of the work in any medium, provided the original work is properly cited. [DOI: 10.1149/1945-7111/ab6eed]

Manuscript submitted December 1, 2019; revised manuscript received January 13, 2020. Published February 3, 2020.

Supplementary material for this article is available online

The growing global demand for energy necessitates efficient, clean, and robust energy conversion technologies. Solid oxide fuel cells (SOFC) have attracted much attention as one such technology due to their unique advantages, which include high conversion efficiency of chemical energy directly into electricity, usable heat generation, and the flexibility to operate on hydrogen, synthesis gas, and hydrocarbon-based fuels. Intermediate temperature SOFCs, operating in the 650 °C–800 °C range, are of particular interest because (1) metallic interconnects can be used, which reduces cost compared to materials required for >800 °C operation, and (2) currently available fuels such as natural gas, propane, and butane are processed in this temperature range.

At intermediate temperatures, the cathode impedance is regularly cited as the primary contributor to SOFC performance losses.⁴ most common cathode is a porous composite of lanthanum strontium manganite (LSM) and yttria-stabilized zirconia (YSZ). LSM provides electronic conductivity for transport of electrons from the external circuit to the active functional layer and catalytic activity for the oxygen reduction reaction within the functional layer. YSZ provides oxygen ion conductivity for transport of oxygen ions from active catalytic sites in the functional layer to the fuel cell electrolyte. Since LSM has negligible ionic conductivity, $< 10^{-8} \, \mathrm{s \cdot cm}^{-1}$, electrocatalytically active sites can only occur at the interface of a percolated network of LSM particles, a percolated network of YSZ particles, and oxygen in the gas phase. Such an interface is called an active three-phase boundary (TPB). The fact that LSM has negligible ionic conductivity severely limits the length of active TPB and, in turn, the density of active sites, particularly in commercial co-sintered cathodes comprising random mixtures of micron sized LSM and YSZ particles.

The limited TPB in LSM-YSZ cathodes led to a large body of research replacing LSM with mixed ionic-electronic conductors (MIECs); the most common being a perovskite with cobalt or a mixture of cobalt and iron in the B-site. Since MIECs have both ionic and electronic conductivity, electrocatalytically active sites

occur anywhere the surface of MIEC particles interface with oxygen in the gas phase, resulting in a higher density of active sites compared to LSM-YSZ. In addition, cobaltites have higher activity due to higher ionic conductivity, electronic conductivity, oxygen diffusivity, and oxygen dissociation compared to other cathode materials. The drawback is that they are highly reactive with YSZ and have a detrimental thermal expansion mismatch with SOFC electrolyte materials. Reactivity with YSZ is often circumvented by adding a ceria-based thin film between the YSZ electrolyte and the cathode. Currently, the state-of-the-art MIEC cathode functional layer is a mixture of $La_xSr_{1-x}Co_yFe_{1-y}O_{3-\delta}$ (LSCF) and $Ce_xGd_{1-x}O_{2-\delta}$ (GDC); however, it has been reported that Sr diffuses out of the perovskite and into the ceria-based barrier layer, degrading performance and causing the cathode to delaminate from the electrolyte. 10,11

An alternative to replacing LSM with MIECs is to decorate the surface of LSM-YSZ composites with MIEC particles, typically by infiltration of metal salts and subsequent calcination. Upon calcination, the infiltrated particle size is typically distributed over a range of 20 nm to 80 nm and does not form percolated particle networks. ^{12–16} Infiltrating LSM-YSZ cathodes with LSCF, cobaltites, and doped cerias have all been shown to lower impedance to the electrocatalytic reaction in the cathode, ^{12–16} and the improvement is attributed to high electrocatalytic activity of the infiltrated particles located near LSM-YSZ active TPBs.

Here we report on the dramatic performance improvement of a commercial SOFC by infiltrating ultra-high surface area nanoYSZ, up to $\sim\!115~\text{m}^2\cdot\text{g}^{-1}$ with an average characteristic particle size of $\sim\!10~\text{nm}$, into the LSM-YSZ cathode. The nanoYSZ was generated via in situ carbon templating, a processing method that our lab has developed. This method produces high surface area mixed-metal-oxides by heating hybrid inorganic-organic materials to 850 °C–1350 °C in nitrogen or argon followed by oxidation at 700 °C in air. $^{17-19}$ As stated previously, nanoYSZ is a pure oxygen ion conductor and has virtually no electrocatalytic activity for the oxygen reduction reaction. Similar to reports on infiltrated MIECs, the addition of nanoYSZ lowered the cathode reaction impedance by 40%. This is attributed to an increased density of active TPB sites in the cathode because the ultra-high surface area nanoYSZ particles

¹National Energy Technology Laboratory, United States of America

²Department of Engineering, Wake Forest University, Winston-Salem, North Carolina 27101, United States of America

³ Center for Functional Materials, Wake Forest University, Winston-Salem, North Carolina 27101, United States of America

⁴Leidos Research Support Team, Morgantown, West Virginia 26507, United States of America

⁵Department of Mechanical and Aerospace Engineering, West Virginia University, Morgantown, West Virginia 26506, United States of America

^{*}Electrochemical Society Member.

^zE-mail: grossmd@wfu.edu

form percolated networks over the LSM-YSZ surface. Remarkably, nanoYSZ also lowered the impedance to bulk charge transport by a massive 35%. Such an improvement in the ohmic impedance is typically not observed with infiltrated MIECs, and can be attributed to broadening the pathway for oxygen ion conduction in the active functional layer. There is one report of infiltrated LSCF improving the ohmic impedance of LSM-YSZ; however, the improvement was overshadowed by a much larger improvement in the reaction impedance.¹⁴ Although we observed that infiltrating a cobaltite with high electrocatalytic activity and oxygen ion conductivity lowered the cathode reaction impedance more than nanoYSZ, the combination of lower reaction and lower bulk charge transport impedance with nanoYSZ resulted in superior performance. While structural stability of nanoparticles is often a point of concern for performance degradation, here we show that the performance of the cell modified with nanoYSZ was three times more stable than that of the cell with PBC ($Pr_xBa_{1-x}CoO_{3-\delta}$). These results bring to light a new approach to improving the electrochemical performance of commercial LSM-YSZ cathodes.

Experimental

Material preparation.—NanoYSZ was generated via an in situ carbon templating processing method, which has also been shown to generate ultra-high surface area particles for other SOFC relevant mixed-metal-oxides including GDC, LSCF, and strontium titanate. 17-20 The in situ carbon templating method involves two steps. First, a hybrid inorganic-organic material containing stoichiometric amounts of metal components of the desired mixed-metaloxide is heat treated at 850 °C-1350 °C in an inert atmosphere such as nitrogen or argon. During this process, the organic component of the hybrid material undergoes pyrolysis, leaving behind amorphous carbon. The amorphous carbon generated in situ becomes a hard template throughout which metal oxide particles are distributed. The carbon template prevents the metal oxide particles from coalescing during high temperature treatment, preserving their nanomorphology. In the second step, the carbon template is removed by low temperature oxidation in air at 700 °C. Oxidation at 700 °C does not cause significant particle coarsening. In our previous works, two types of hybrid inorganic-organic materials were used: (1) propylene oxide gels with a glucose additive (POG) and (2) citric acid gels (CA). The carbon concentrations and final surface areas of the mixed-metal-oxides were controlled by varying the concentrations of glucose and citric acid for POG and CA gels, respectively.

In this study, we simplified the formulation of the POG hybrid material by omitting the propylene oxide and, thus, only using glucose and salts of Zr and Y as precursors. This new hybrid material is referred to as YSZ-Glucose and it was prepared by dissolving ZrCl₄ (99.5+%, Alfa Aesar), Y(NO₃)₃•6H₂O (99.9%, Alfa Aesar), and glucose (≥99.9%, Alfa Aesar) in deionized water with a Zr:Y:Glucose:H₂O molar ratio of 5.75:1:30:325. The solution was then heated to 120 °C until all of the water evaporated and a black viscous material formed. The hybrid material (YSZ-Glucose) was then heated in N₂ at 850 °C for 2 h, pyrolyzing the glucose component and resulting in an amorphous composite of nanoYSZ and carbon. The composite was subsequently calcined in air at 700 °C for 2 h, which oxidized the amorphous carbon and formed nanoYSZ.

Material characterization.—The phase compositions of the YSZ-Glucose heated in N_2 and subsequently calcined in air were identified with powder X-ray diffraction (PXRD). The experiments were conducted at ambient temperature using a Bruker D2 Phaser diffractometer with CuKα radiation and a 2θ ranging between 25° and 65°. The carbon template concentration was determined via thermogravimetric analysis (TGA) using a TA Instruments SDT Q600. In this experiment, YSZ-Glucose that had been heat treated in N_2 was heated from ambient temperature to 1200 °C at a 10 °C·min $^{-1}$ ramp rate in air flowing at 100 cm 3 ·min $^{-1}$, and the

weight loss due to carbon oxidation was used to determine the carbon concentration. The nanoYSZ specific surface area was determined by the Brunauer, Emmett, Teller (BET) method. The experiment was conducted with a Micromeritics Tristar II 3020 surface area analyzer with nitrogen adsorption at 77 K. The sample was degassed at 250 °C for 2 h before testing and the correlation coefficient of the reported surface area was > 0.9995. The structure of nanoYSZ was characterized with transmission electron microscopy (TEM). Electron diffraction, diffraction contrast, and high resolution TEM imaging were performed using a JEM-2100 operated at 200 kV.

Fuel cell modification.—The fuel cells used in this study were produced by MSRI and consisted of a 10 μ m thick YSZ electrolyte, a Ni-YSZ anode with a 750 μ m thick support current collecting layer and a 10 μ m thick functional layer, and an LSM-YSZ cathode with a 40 μm thick current collecting layer and a 10 μm thick functional layer. One cell was modified with nanoYSZ by infiltrating the cathode once with an aqueous solution of ZrCl₄, Y(NO₃)₃•6H₂O, and glucose. The cell was then heated to 850 °C in N2 for 2 h. After heating in N₂, the cathode pores contained a mixture of nanoYSZ and amorphous carbon. The cell was subsequently calcined in air at 700 °C for 2 h to remove the amorphous carbon, resulting in nanoYSZ decorating the surface of the LSM and YSZ scaffold particles. The LSCF modified cell was prepared by infiltrating an aqueous solution containing glucose, propylene oxide, and nitrates of La, Sr, Co, and Fe into the LSM-YSZ cathode. The cell was then heated to 850 °C in N₂ and subsequently oxidized at 700 °C in air. The PBC modified cell was prepared by infiltrating an aqueous solution containing nitrates of Pr, Ba, Co, and citric acid (CA) with a Pr:Ba:Co:CA molar ratio of 0.5:0.5:1:2 into the LSM-YSZ cathode. After infiltration, the cell was heated to 850 °C in air to form the desired PBC phase. The nanoYSZ, LSCF, and PBC loadings in the cathode were 4.2 wt%, 2.6 wt%, and 10.0 wt%, respectively.

Fuel cell characterization.—The electrochemical performances of the baseline cell and the cells modified with nanoYSZ, LSCF, and PBC were evaluated using Electrochemical Impedance Spectroscopy (EIS) and current-voltage (i-V) measurements. The potentiostat/ galvanostat (Solartron 1470E) and a frequency response analyzer (Solartron 1455 A) with four probes were used to conduct the experiments. Pt mesh/Pt paste and Pt mesh/Ni paste were used for current collection at the cathode and anode, respectively. All fuel cell tests were conducted at 750 °C. Hydrogen gas was used as fuel in the anode and air was used as the oxidant gas in the cathode. Both gases were flowing at 300 cm³·min⁻¹. For EIS, the data were collected in galvanostatic mode with a 1.0 A·cm⁻² dc current, 10 mA ac perturbation, and a frequency ranging between 10⁵ and 0.05 Hz. The resulting impedance spectra were deconvoluted by non-linear least squares regression using Zview software. The morphologies of the baseline cathode and the modified cathodes were examined after fuel cell performance testing with a scanning electron microscope (JEOL, JSM-7600F).

Results and Discussion

As indicated by powder X-ray diffraction (PXRD), a pure YSZ phase is obtained upon heating and subsequently calcining YSZ-Glucose at 850 °C in N_2 and 700 °C in air, respectively (Fig. S1, Supplementary Information, available online at stacks.iop.org/JES/167/024517/mmedia). The PXRD peaks are broad and the nanoYSZ crystallite size, estimated using the Scherrer equation, is \sim 8 nm. The nanoYSZ surface area was determined to be $116 \, \mathrm{m}^2 \cdot \mathrm{g}^{-1}$ (Fig. S2, Supplementary Information). This surface area corresponds to a characteristic particle size of \sim 9 nm, assuming spherical particles of the same size. The estimated particle size and crystallite sizes are similar, suggesting that the individual particles are not polycrystalline.

Transmission electron microscopy (TEM) images of the YSZ-Glucose heated in N₂ at 850 °C and subsequently calcined in air at

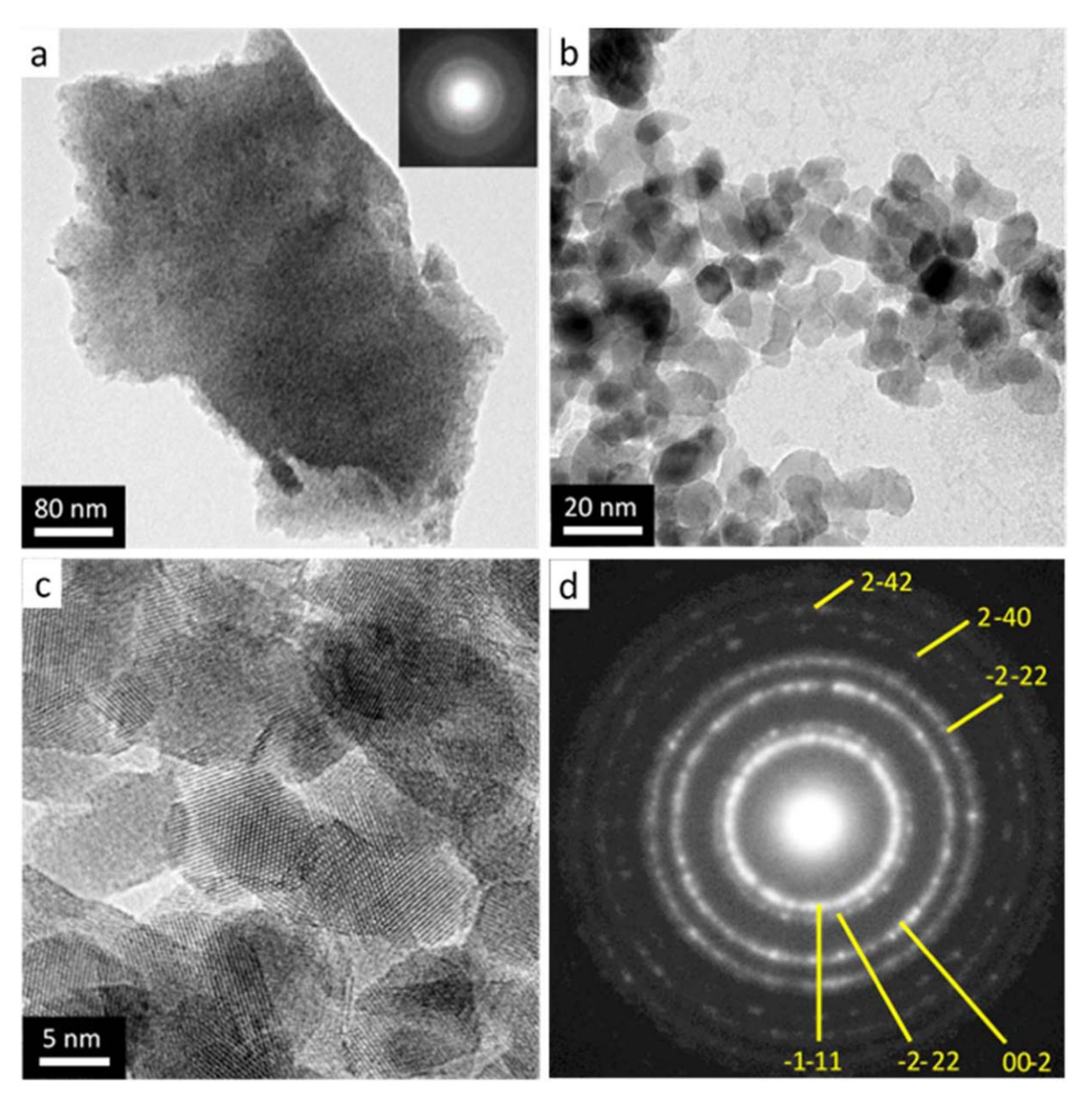


Figure 1. TEM images of YSZ-Glucose (a) heated to 850 °C in N_2 and (b)–(c) subsequently calcined in air at 700 °C. (c) Zoomed in view of (b). (d) TEM electron diffraction ring of YSZ nanoparticles (depicted in (c) with a cubic crystal structure.

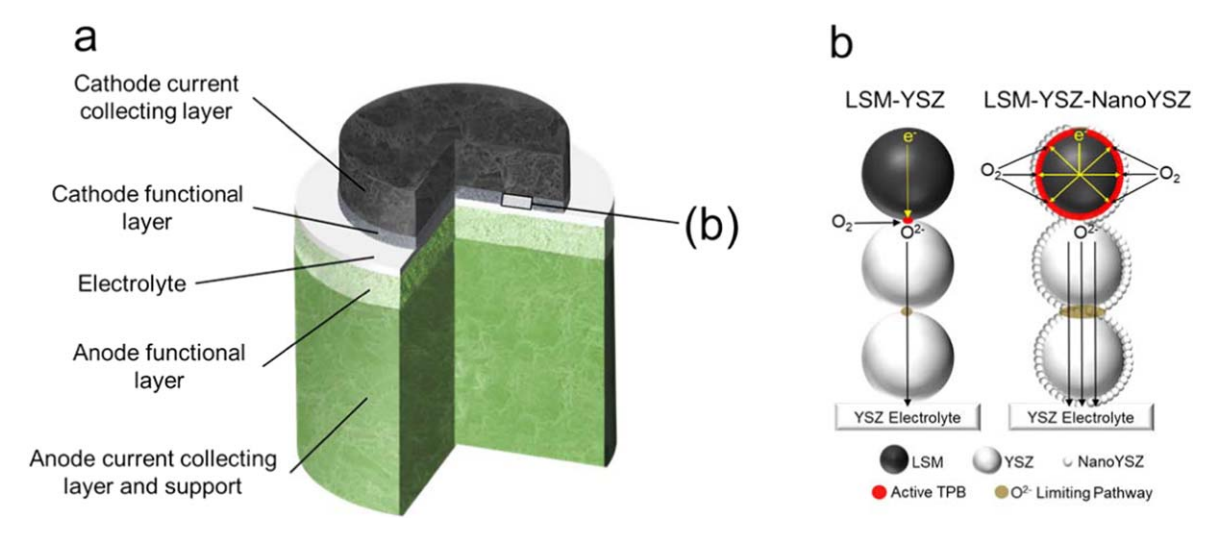


Figure 2. Schematic image of (a) a commercial MSRI cell showing its different structural layers and (b) the proposed effect of incorporating nanoYSZ into the cathode.

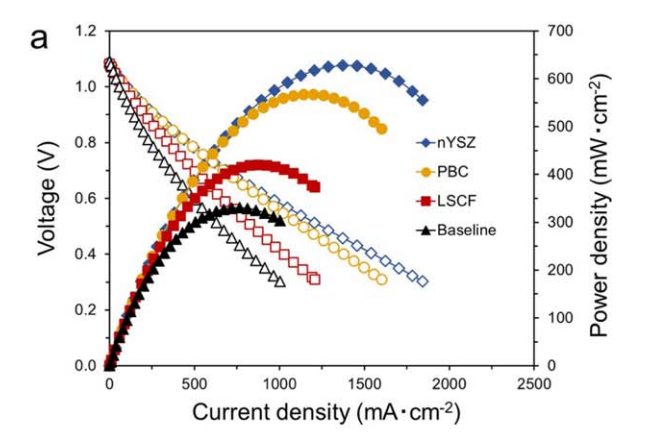
700 °C are shown in Fig. 1. The diffraction pattern in Fig. 1a indicates the formation of an amorphous material upon heating in N_2 . Thermogravimetric analysis (TGA) in flowing air indicates that \sim 68 wt% of the amorphous sample is carbon (Fig. S3, Supplementary Information). Oxidation of the carbon template at 700 °C leaves behind discrete YSZ nanoparticles with a characteristic size between \sim 5 nm and \sim 10 nm (Figs. 1b and 1c). The diffraction pattern of these particles is shown in Fig. 1d and indicates that a pure, crystalline YSZ cubic structure forms.

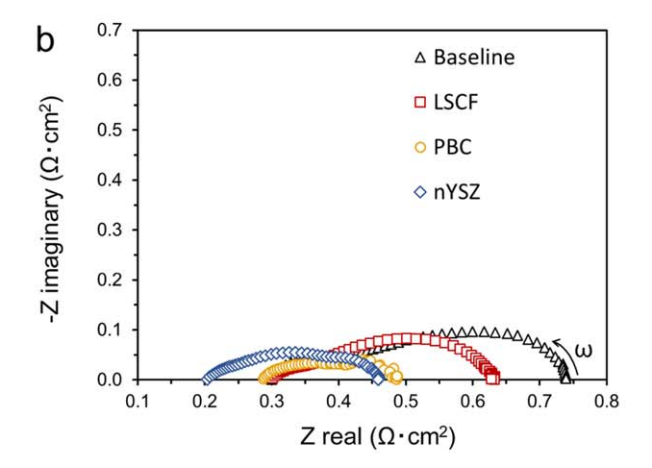
Upon establishing that pure, ultra-high surface area nanoYSZ can be obtained with YSZ-Glucose, the impact of integrating nanoYSZ into commercial LSM-YSZ cathodes was considered. The studied commercial SOFCs were manufactured by Materials & Systems Research Inc. (MSRI). A schematic of the SOFC structural components and the proposed impact of nanoYSZ on the cathode functional layer performance are shown in Fig. 2. The cathode functional layer comprises a mixture of LSM and YSZ particles with a characteristic size of order 1 μ m. The nanoYSZ particles added to the cathode, which are two orders of magnitude smaller than the LSM and YSZ scaffold particles, are expected to form an interconnected network of particles on the surface of both LSM and YSZ particles as illustrated in Fig. 2b. 21,22 This percolated network provides (1) additional active TPB reaction sites at the interface of nanoYSZ and LSM particles and (2) broader O2- conduction pathways in the YSZ phase. The higher TPB density is expected to lower the impedance to the cathode reaction and the broader O² pathways are expected to lower the impedance to bulk charge transport. Ultimately, both lower the overall impedance and increase the power density of the fuel cell.

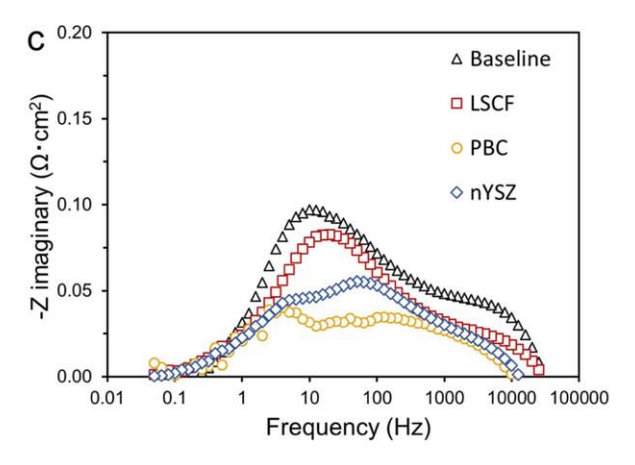
The proposed impact of adding nanoYSZ to a commercial cathode is tested by comparing fuel cell performance of a baseline MSRI cell and an MSRI cell modified with nanoYSZ. Fuel cell performances of MSRI cells modified with two MIECs, LSCF and PBC, were also collected for comparison. The fuel cell performance data reported in Fig. 3 were collected after 24 h of continuous operation for all cells. As shown in Fig. 3a, the cell modified with nanoYSZ has the highest maximum power density (628 mW·cm⁻²), a 90% increase over the baseline cell (330 mW·cm⁻²). Compared to cells modified with MIECs, the nanoYSZ cell maximum power density is 50% higher than LSCF and 11% higher than PBC. Remarkably, nanoYSZ achieves the highest maximum power density, despite having no inherent activity for the oxygen reduction reaction and only O²⁻ conductivity as its singular function.

To explain the striking impact of nanoYSZ on cell performance, electrochemical impedance spectroscopy (EIS) was performed on the cells. The Nyquist plot in Fig. 3b shows that the polarization resistance is substantially lower than the baseline cell for all three modified cells. The polarization resistance is equal to the difference between the low frequency and high frequency intercepts with the abscissa on the Nyquist plot. LSCF, PBC, and nanoYSZ reduce the polarization resistance by 24% from 0.44 $\Omega \cdot \text{cm}^2$ to 0.33 $\Omega \cdot \text{cm}^2$, 53% to 0.21 $\Omega \cdot \text{cm}^2$, and 40% to 0.27 $\Omega \cdot \text{cm}^2$, respectively. Bode plots in Fig. 3c show that the maxima in the frequency range of 10 Hz—150 Hz are lower for all three modified cells, which typically corresponds to a reduction in cathode activation polarization. Equivalent circuit modeling of the impedance spectra (Section 2, Supplementary Information) suggests that the infiltrates dominantly improve oxygen surface adsorption kinetics. 25

Although PBC lowers the cathode polarization impedance the most, the nanoYSZ modified cell is the only one with a significantly reduced ohmic resistance. The ohmic resistance corresponds to the high frequency intercept with the abscissa on the Nyquist plot in Fig. 3b. LSCF and PBC lower the ohmic resistance by 0.2% from 0.300 Ω ·cm² to 0.299 Ω ·cm² and 6.2% to 0.281 Ω ·cm², respectively. However, nanoYSZ reduces the ohmic resistance by an immense 35% from 0.300 Ω ·cm² to 0.195 Ω ·cm². This suggests that the addition of nanoYSZ significantly enhances the bulk transport of charged species in the cathode. Considering YSZ is an O²-conductor and an electronic insulator, the improvement in ohmic







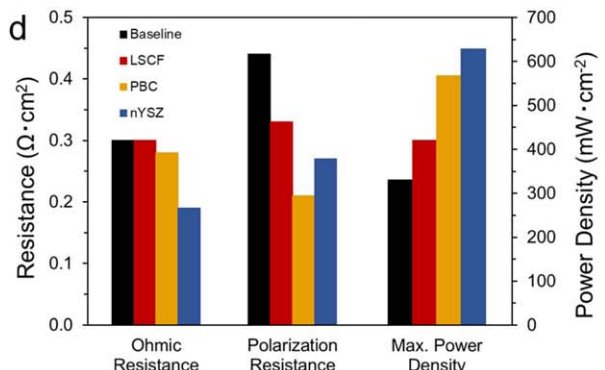


Figure 3. (a) Fuel cell *i-V-P* performance, (b) Nyquist plots, and (c) Bode plots of the studied commercial cells. (d) Ohmic resistance, polarization resistance, and maximum power density of the studied commercial cells. All fuel cell performance data were collected at 750 °C.

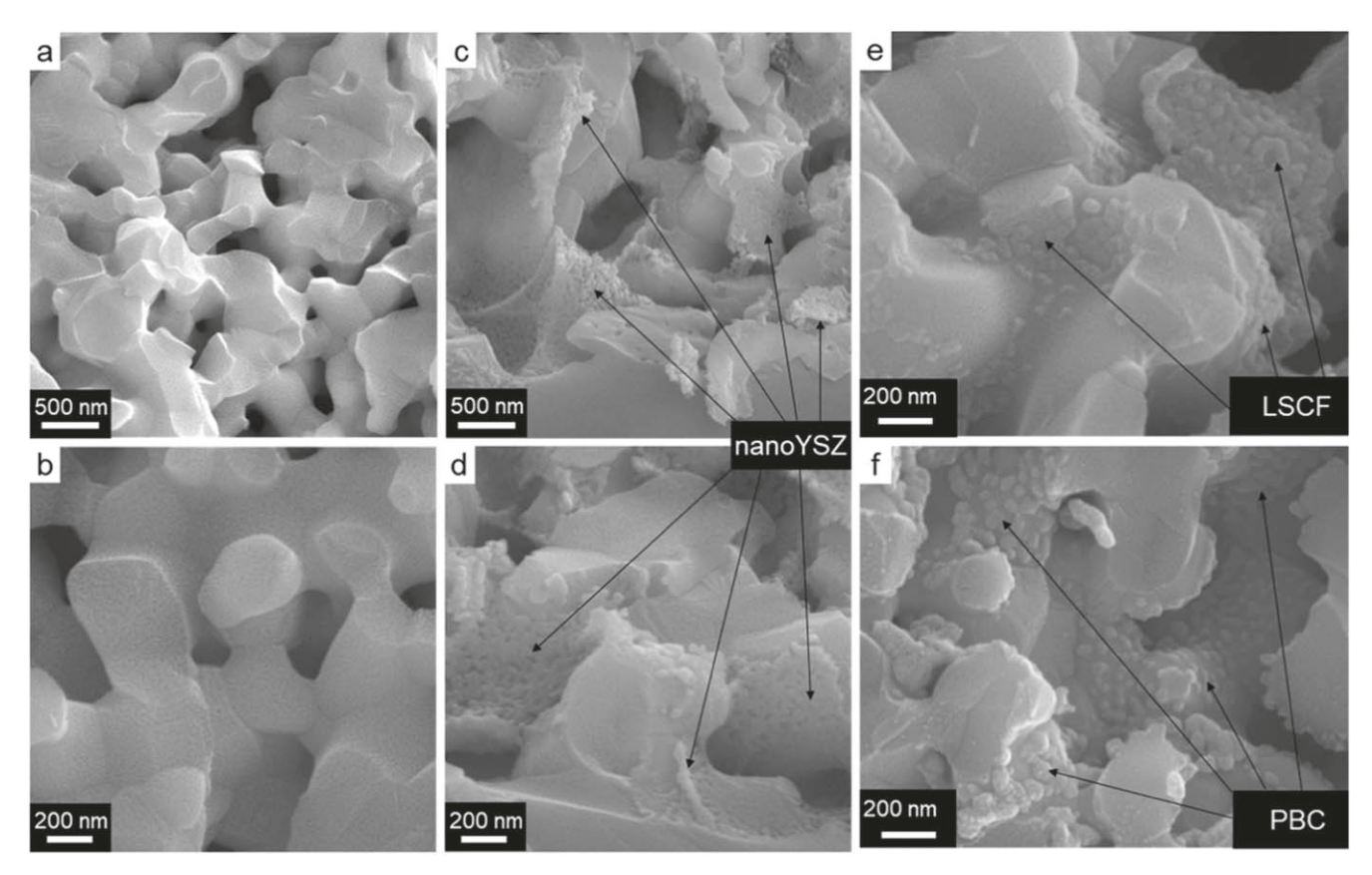


Figure 4. SEM images of commercial LSM-YSZ cathodes without modification (a) and (b), with nanoYSZ (c) and (d), with LSCF (e), and with PBC (f).

resistance can be attributed to improving bulk transport of O^{2-} in the cathode. 26

A summary of the ohmic resistance, polarization resistance, and maximum power density for all four cells is shown in Fig. 3d. Considering cobaltites have higher activity for the oxygen reduction reaction than YSZ and LSCF, it is not surprising that the PBC modified cell has the lowest cathode polarization impedance. It is surprising, however, that the nanoYSZ lowers the polarization impedance more than LSCF because YSZ has no inherent activity for the oxygen reduction reaction. Furthermore, given that the $\rm O^{2-}$ conductivity of LSCF, PBC, and YSZ are all similar at 750 °C, $\sim \! 0.03 \, \rm s \cdot cm^{-1}, ^{27-29}$ it is interesting that a large improvement in ohmic resistance only occurs with nanoYSZ.

In an attempt to explain these differences in fuel cell performance, cross sectional scanning electron microscopy (SEM) images of the cathode functional layer for all four cells were compared post fuel cell testing. Figure 4 shows cathode SEM images of the baseline cell and the cells modified with nanoYSZ, LSCF and PBC. As the figure shows, the nanoYSZ cell forms an interconnected network of YSZ nanoparticles on the surface of the LSM-YSZ porous scaffold (Figs. 4c and 4d) that are not present in the baseline cell (Figs. 4a and 4b). The characteristic size of the YSZ nanoparticles ranges from ~ 10 nm to ~ 30 nm and the particles are evenly distributed over the porous scaffold, suggesting that the YSZ nanoparticles decorate the surface of both LSM and YSZ scaffold particles. The LSCF particles in the cathode functional layer are larger than nanoYSZ, with a characteristic size between 30 nm and 60 nm, and do not form percolated networks as extensively as nanoYSZ (Fig. 4e). The PBC particles are even larger, ranging from 50 nm to 100 nm, and form percolated networks of particles to an even lesser degree (Fig. 4f).

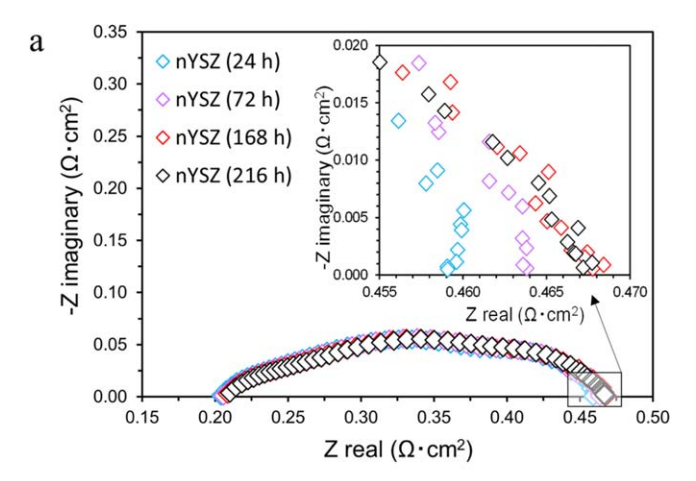
The unique morphology of nanoYSZ in the SEM images supports the proposed and observed impact of nanoYSZ on cathode performance. In regards to the improvement in ohmic resistance, it is possible for variations in electrolyte thickness to account for variations in ohmic resistance; however, differences in electrolyte thickness and, in turn, electrolyte ohmic resistance between the tested cells was determined to be negligible (Section 3, Supplementary Information). Thus, the significant improvement in ohmic resistance can be explained by the robust network of interconnected nanoYSZ particles, which broadens the ${\rm O}^{2-}$ conduction pathways within the cathode functional layer. Assuming the effective ${\rm O}^{2-}$ conductivity of YSZ scaffold particles is 2% of bulk YSZ, as reported in the literature, $^{21,30}_{21,30}$ a 35% reduction in ohmic resistance corresponds to nanoYSZ tripling the effective ${\rm O}^{2-}$ conductivity to 6% of the bulk (Section 4, Supplementary Information).

The formation of percolated nanoYSZ particle networks is also critical to lowering the cathode polarization impedance. Percolated nanoYSZ particles in the cathode functional layer that are in contact with LSM are active TPB reaction sites. Thus, the combination of small nanoparticles and the formation of an interconnected network results in a large increase in active TPB sites and a significant decrease in cathode polarization impedance.

In the case of MIECs, the small extent to which LSCF and PBC particles formed percolated networks aligns with the small improvements in ohmic resistance that are observed experimentally. In regards to polarization impedance, MIEC particles in contact with YSZ scaffold particles can only be active when they have a connection to the electronic conducting phase, LSM. Otherwise, no electronic charge can reach the MIEC particles. Similarly, MIEC particles in contact with LSM scaffold particles can only be active when they have a connection to the oxygen ion conducting phase, YSZ. Otherwise, no oxygen ions can reach the electrolyte. Thus, MIEC particles can only improve cathode polarization resistance near existing LSM-YSZ active TPB sites and along percolated networks of MIEC particles that span LSM and YSZ. Both contribute to a lower polarization impedance; however, the majority of improvement is

likely due to enhancing existing active sites given the low extent to which interconnected MIEC particle networks formed.

The superior performance of nanoYSZ modified cells is a promising finding; however, the degradation of fuel cell performance over time is a critical challenge for commercial cells and the stability of nanoparticles at SOFC operating temperatures is a common concern. To address these issues, we monitored fuel cell performance over 230 h by continuously recording voltage and current over time and intermittently collecting impedance measurements. Figure 5a shows that after 216 h of continuous operation, the total resistance of the nanoYSZ modified cell only increases by 1.4% from 0.460 $\Omega \cdot \text{cm}^2$ to 0.468 $\Omega \cdot \text{cm}^2$. The corresponding maximum power density only decreases by 2.2% from 628 mW·cm⁻² to 614 mW⋅cm⁻² over the same period of time, Fig. 5b. For comparison, the PBC modified cell operated for only 120 h shows an increase in total resistance of 4.1% from 0.487 Ω -cm² to $0.507~\Omega\cdot cm^2$ and a 3.7% decrease in maximum power density from 567 mW·cm $^{-2}$ to 546 mW·cm $^{-2}$ (Fig. S7, Supplementary Information). In addition, continuous voltage measurements conducted on both the PBC and nanoYSZ modified cells further confirm that the PBC cell degrades at a higher rate than the nanoYSZ cell (Fig. S8, Supplementary Information). The PBC cell voltage decreases at a rate of 0.73%/100 h, a rate more than three times higher than that of the nanoYSZ cell (0.23%/100 h). The faster rate of degradation with the PBC modified cell is most likely due to a reduction in active TPB site density by (1) particle coarsening or (2) reaction with the YSZ scaffold particles, both of which are common problems with cobaltites. The nanoYSZ cell, on the other hand, does not face the chemical reactivity issue and, based on our



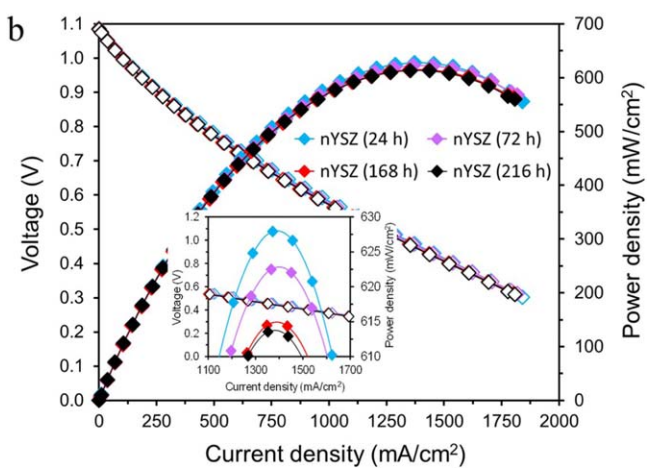


Figure 5. long-term performance stability of the commercial LSM-YSZ cell with nanoYSZ. (a) Nyquist plots and (b) fuel cell *i-V-P* data were collected at different fuel cell operation times.

previous works, YSZ nanoparticles prepared via in situ carbon templating can maintain their nanostructure for long periods of time (>2000 h).

Conclusions

We have successfully prepared ultra-high surface area nanocrystalline YSZ within commercial LSM-YSZ SOFC cathodes using an in situ carbon templating processing method. Modifying commercial cells with nanoYSZ increased maximum power density by 90%, which outperformed cells modified with two MIECs: LSCF and PBC. The massive increase in power density was attributed to the formation of robust interconnected networks of YSZ nanoparticles, improving the cathode catalytic activity by 40% and bulk charge transport by 35%. In comparison, MIECs significantly improved cathode catalytic activity, but only showed slight improvement in bulk charge transport. SEM images suggest MIECs had little impact on cell ohmic resistance because the nanoparticles were larger than nanoYSZ and did not form significant networks of interconnected particles. As a result, nanoYSZ enhanced the density of active TPB sites and enlarged the ionic conduction pathways more extensively than the MIECs. Finally, the nanoYSZ cell performance was found to be three times more stable than the PBC cell. The results demonstrate that in situ carbon templating of nanoYSZ provides a new approach to improving the performance and stability of commercial LSM-YSZ cathodes.

Acknowledgments

This work was supported by the National Science Foundation Faculty Early Career Development (CAREER) award (CMMI-1651186) and the National Energy Technology Laboratory's ongoing research under the RSS Contract 89243318CFE000003.

References

- K. Kendall and M. Kendall, in High-Temperature Solid Oxide Fuel Cells for the 21st Century: Fundamentals, Design and Applications (Academic, Cambridge, MA, USA) 2, p. 1 (2015).
- 2. E. D. Wachsman and K. T. Lee, Science, 334, 935 (2011).
- K. Kendall and M. Kendall, in High-Temperature Solid Oxide Fuel Cells for the 21st Century: Fundamentals, Design and Applications (Academic, Cambridge, MA, USA) 2, p. 42 (2015).
- 4. J. M. Vohs and R. J. Gorte, Adv. Mater., 21, 943 (2009).
- X. Zhang, L. Liu, Z. Zhao, B. Tu, D. Ou, D. Cui, X. Wei, X. Chen, and M. Cheng, Nano Lett., 15, 1703 (2015).
- T. Z. Sholklapper, C. P. Jacobson, S. J. Visco, and L. C. DeJonghe, Fuel Cells, 5, 303 (2008).
- K. Kendall and M. Kendall, in High-Temperature Solid Oxide Fuel Cells for the 21st Century: Fundamentals, Design and Applications (Academic, Cambridge, MA, USA) 2, p. 161 (2015).
- S. K. Burnwal, S. Bharadwaj, and P. Kistaiah, J. Mol. Eng. Mater., 4, 163001 (2016).
- 9. C. Sun, R. Hui, and J. Roller, J. Solid State Electr., 14, 1125 (2010).
- 10. F. Tietz, A. Mai, and D. Stover, Solid State Ion., 179, 1509 (2008).
- S. P. Simner, M. D. Anderson, M. H. Engelhard, and J. W. Stevenson, *Electrochem. Solid-State Lett.*, 10, A478 (2006).
- D. Ding, X. Li, S. Y. Lai, K. Gerdes, and M. Liu, *Energy Environ. Sci.*, 7, 552 (2014).
- R. Kiebach, C. Knofel, F. Bozza, T. Klemenso, and C. Chatzichristodoulou, *J. Power Sources*, 228, 170 (2013).
 Q. S. Zhang, A. Hirano, T. Matsumura, N. Imanishi, Y. Takeda, and K. Yamahara,
- J. Fuel Cell Sci. Tech., 6, 011010 (2009).

 15. C. Lu, R. Sholklapper, C. P. Jacobson, S. J. Visco, and L. C. DeJonghe,
- J. Electrochem. Soc., 1536, A1115 (2006).
 X. Li, N. Xu, X. Zhao, and K. Huang, J. Power Sources, 199, 132 (2012).
- S. P. Muhoza, T. E. Barrett, M. A. Cottam, S. E. Soll, M. D. Yuce, V. S. Prathab, S. K. Hambright, M. Rezazad, O. Racchi, and M. D. Gross, *J. Electrochem. Soc.*, 1652, F46 (2018).
- S. P. Muhoza, A. McCormack, R. W. Garrett, M. D. Yuce, V. S. Prathab, S. K. Hambright, M. A. Cottam, and M. D. Gross, *J. Electrochem. Soc.*, 1662, F53 (2019).
- 19. S. P. Muhoza, M. A. Cottam, and M. D. Gross, *J. Vis. Exp.*, **122**, e55500 (2017).
- M. A. Cottam, S. P. Muhoza, and M. D. Gross, J. Am. Ceram. Soc., 99, 2625 (2016).
- M. J. Synodis, C. L. Porter, N. M. Vo, A. J. L. Reszka, M. D. Gross, and R. J. Snyder, *J. Electrochem. Soc.*, 160, F1216 (2013).
- A. J. L. Reszka, R. C. Snyder, and M. D. Gross, *J. Electrochem. Soc.*, 161, F1176 (2014)

Journal of The Electrochemical Society, 2020 167 024517

- S. Lee, N. Miller, and K. Gerdes, J. Electrochem. Soc., 159, F301 (2012).
 C. Endler, A. Leonide, A. Weber, F. Tietz, and E. Ivers-Tiffee, J. Electrochem. C. Elidiet, A. Leolide, A. Weber, F. Herz, and E. Ivels-Hill Soc., 157, B292 (2010).
 T. Yang et al., J. Electrochem. Soc., 166, F448 (2019).
 Y. Chen, K. Gerdes, and X. Song, Sci. Rep., 6, 32997 (2016).

- B. Fan, J. Yan, and X. Yan, *Solid State Sci.*, 13, 1835 (2011).
 K. Zhang, L. Ge, R. Ran, Z. Shao, and S. Liu, *Acta Mater.*, 56, 4876 (2008).
 K. Sasaki and J. Maier, *Solid State Ion.*, 134, 303 (2000).
 K. Yamahara, T. Z. Sholklapper, C. P. Jacobson, S. J. Visco, and L. C. De Jonghe, *Solid State Ion.*, 176, 1359 (2005).